Tetrabutylphosphonium Cation as a Template in the Kinetics of the Crystallization of B-ZSM-5

Vedachalam Sundaramurthy and Nachiappan Lingappan*

Department of Chemistry, Anna University, Chennai-600025, India

(Received March 16, 1999)

Pentasil zeolite, B-ZSM-5 and Al-ZSM-5, have been synthesized hydrothermally using orthoboric acid and sodium aluminate, respectively, with ethyl silicate-40 so as to obtain a gel mix with $SiO_2/M_2O_3 = 22$ (where M = B or Al) employing a tetrabutylphosphonium bromide (TBPBr) template at temperatures of 423, 448, and 473 K. The crystallization kinetics followed by XRD, FTIR, and SEM studies clearly demonstrate the influence of the size of the hetero atoms on the rate of nucleation and crystallization. The values of the apparent activation energies for nucleation and crystal growth indicate that both nucleation and crystal growth are faster for the Al-ZSM-5 system than for the B-ZSM-5 system. Avrami–Erofeev parameters for both systems have been evaluated. Correlations were found between the kinetics of crystallization and the characteristics of the formed crystal. SEM pictures show similar, but larger sized, crystals for the Al-ZSM-5 system than those of the B-ZSM-5 system. XRD, FTIR, and chemical analysis have revealed that the mechanism operating during crystallization is the same, and that hetero atoms become incorporated with the framework during the nucleation step, itself, with boron at a slower rate.

Zeolites whose silica frameworks contain substituents other than aluminium are found in nature.[1] Such structures can be prepared in the laboratory, either by crystallization[1,2] or by framework modification with various reagents.[3] A more frequently mentioned zeolite in this regard, particularly in the patent literature, is boron containing the pentasil zeolite ZSM-5 (a boralite). In boralite, boron occupies the typical site of the framework aluminium. The incorporation of boron in pentasil zeolite (MFI and MEL) structures has been claimed since 1978. Evidence for this substitution was obtained from measurements of the size of the unit cell[4] and from magic-angle spinning (MAS) NMR data.[5,6] In the preparation of B-ZSM-5 (B-MFI), mainly the tetrapropylammonium cation[4,7—10] and alkylamines[11] are being used. B-ZSM-11, another boralite with the MEL structure, is being prepared using the versatile tetrabutylammonium hydroxide (TBA) as a template.[12,13] Using the tetrabutylphosphonium cation (TBP), pure Al-ZSM-5 has been reported for the first time under specific synthetic conditions using a polymeric silica source[14] instead of the common monomeric silica source. The literature shows that most of the work on boralite has been devoted to its synthesis, characterization[12,15—17] and reactions.[18—22] The kinetics part of their crystallization still remains insufficiently examined. It was therefore thought worthwhile to examine the kinetics of both the process of nucleation and crystallization of MFI boralite using the TBP template itself. In this study we compared the rates of nucleation and crystallization of the B-ZSM-5 and Al-ZSM-5 zeolites from the their gel mix containing a SiO_2/M_2O_3 ratio of 22 (M = B or Al) using the tetrabutylphosphonium (TBP) cation template in separate batches; also, the influence of the temperature on the rates of crystallization was studied. The activation energy for nucleation and crystallization and the Avrami–Erofeev parameters were determined so as to understand the crystallization mechanism.

Experimental

The materials used for synthesis runs were ethyl silicate-40 (Pentameric silicate ester containing SiO_2 40% by wt, Mettur Chemicals, S.India), sodium aluminate (Anala R), orthoboric acid (Anala R), tetrabutylphosphonium bromide (TBPBr) (E. Merck), sodium hydroxide (Anala R), and demineralized water.

The experiments were performed using gel mixtures of molar composition, 0.48 TBPBr : 4.1 Na_2O : M_2O_3 : 22 SiO_2 : 735 H_2O (where M = B or Al). In a typical experiment, 40 g of ethyl silicate-40 was diluted with 50 ml of deionized water and stirred mechanically for one hour to obtain solution A. After orthoboric acid 1.5 g (or 2.6 g of sodium aluminate) was dissolved in 50 ml of water, tetrabutylphosphonium bromide (2 g in 5 ml of water) was slowly added to it with stirring to obtain solution B. Solution B was added to solution A with constant stirring. A solution of sodium hydroxide (3.2 g in 40 ml of water) was added in a thin stream to obtain gel mix of pH 9.5±0.2. The thus-obtained gel mix was transferred into a 300 ml capacity steel autoclave and held at a temperature of 448 K in an air oven. At fixed time intervals the reaction vessel was taken out from the thermostat, and the products were removed, washed with distilled water, dried at 393 K, and finally calcined at 823 K for 5 h. X-Ray diffraction patterns of the M-ZSM-5 in a powder form were collected on a Rigaku X-Ray diffractometer with Ni-filtered Cu $K\alpha$ radiation. The percentage crystallinity was estimated[23] based on the ratio of a peak area of 2θ = 22—25° peaks of the solid product to that of the reference sample of ZSM-5 with 100% crystallinity.

The size and shape of the crystals were examined using a scanning electron microscope (SEM; JEOL 2000 JS model) after coating with evaporated Au film. The composition of the intermediates and

final samples were obtained by chemical analysis. Silica was determined gravimetrically. Aluminium, boron and phosphorous were determined using inductive coupled plasma (ICP) analysis. The organic cation present in the zeolite was calculated from the phosphorous content by assuming that one mole of TBP corresponds to one mole of phosphorous.

Results and Discussion

X-Ray diffraction and SEM pictures of the intermediates and final products of synthesis confirm the formation and development of only the MFI-type zeolite phase during the crystallization period. A typical X-ray pattern of B-ZSM-5 synthesized from a gel mixture containing SiO_2/B_2O_3 = 22 is shown in Fig. 1. The crystallization kinetics of M-ZSM-5 (M = Al and B) using the TBP cation in the reaction temperature range 423—473 K are illustrated in Fig. 2. The TBP cation plays a structure-directing role during nucleation by arranging silica tetrahedra in an orderly manner. The crystallization curves indicate a considerable influence of the reaction temperature on the kinetics of the crystallization process. The sigmoidal nature exhibited by the crystallization curves is characteristic of a process involving two distinct stages:[24] (a) an induction period when nuclei are formed; and (b) a crystal-growth period when nuclei grow into crystals. Following the course of crystallization by examining the X-ray diffraction pattern of the solid as a function of the crystallization time provides information about the induction period and crystal-growth period. If it is assumed that the rate of nucleation is inversely proportional to the induction period, then it is evident from the Fig. 2 that the rate of nucleation decreases as the crystallization temperature decreases. It is also clear from Fig. 2 that the rate of crystal growth increases with the crystallization period and passes through the maximum rate at 50—70% of the total crystallinity followed by a slow increase while approaching 100% crystallinity. The higher rates of nucleation and crystal growth at a higher reaction temperature suggest the enhanced solubility of the aluminosilicate (or borosilicate) gel on increasing the crystallization temperature, which exerts a beneficial effect on the crystallization process.[25] The curves in Fig. 2 show that the higher is the temperature the faster is the rate of nucleation and crystallization, irrespective of the nature of the substituent atoms in the framework that is forming.

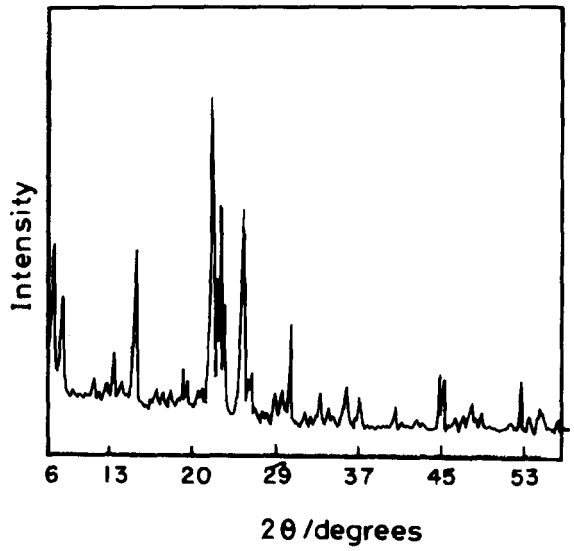

Fig. 1. Typical XRD of B-ZSM-5.

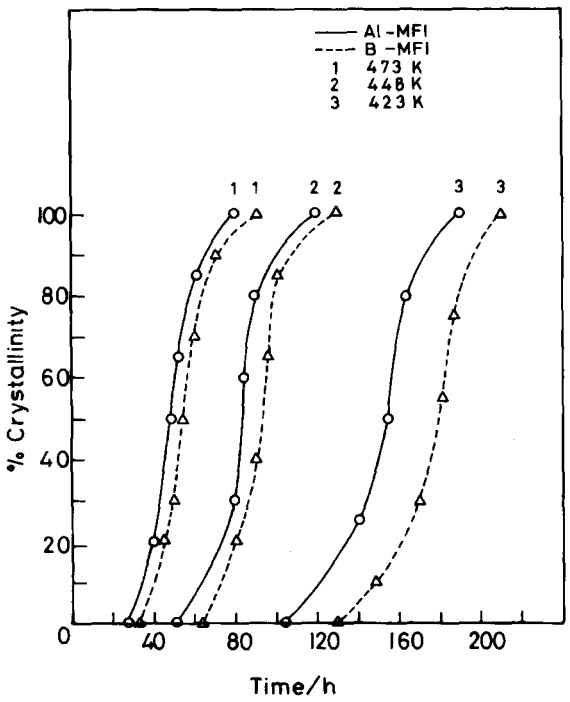

Fig. 2. Crystallization curves for B-ZSM-5 and Al-ZSM-5 systems.

Assuming that the formation of nuclei stable enough not to redisolve, but to grow into a crystal, is an energetically activated process, since nucleation is the rate-determining step during the induction period, the apparent activation energy for nucleation (E_n) was calculated from the temperature dependence of the rate of nucleation,

$$\frac{d\ln 1/\theta}{d1/T} = \frac{-E_n}{R}, \quad (1)$$

where θ is the induction time i.e. the point on the crystallization curve where the conversion to the crystalline phase is just starting and T is the absolute temperature. Similarly, E_c, the apparent activation energy for crystal growth, was calculated from the temperature dependence of the rate of crystallization. The crystallization rate[26] is defined as the rate of conversion at 50% of the total conversion level in terms of the percent conversion per hour,

$$\frac{d\ln 1/\theta}{d1/T} = \frac{-E_c}{R}, \quad (2)$$

where θ is the time taken for 50% crystallization, which does not include the induction period. Linear plots obtained by applying the Arrhenius equation to the crystallization curves are shown in Fig. 3. The activation energy for the nucleation (E_n) values derived from these plots are summarized in Table 1. E_n and E_c, found to be higher for the B-MFI system than for the Al-MFI system, suggest that nucleation

Table 1. Activation Energy of Nucleation (E_n) and Crystallization (E_c)

System[a)]	Source of organic	SiO_2/M_2O_3	E_n/kJ mol^{-1}	E_c/kJ mol^{-1}
B-ZSM-5 (present study)	TBP-Br	22	48.7	39.1
Al-ZSM-5 (present study)	TBP-Br	22	43.1	45.6
Al-ZSM-5[26]	TPA-Br	90	134.4	76.5
Al-ZSM-5[23]	TPA-Br	111	35	166
Al-ZSM-5[27]	TPA-OH	28	107	81
Al-ZSM-5[27]	TPA-Br	90	35.5	83.6
Al-ZSM-5[28]	TPA-Br	70	25	29
ZSM-5[28]	TPA-Br	Al free	38	46

a) Superscripts given are reference numbers.

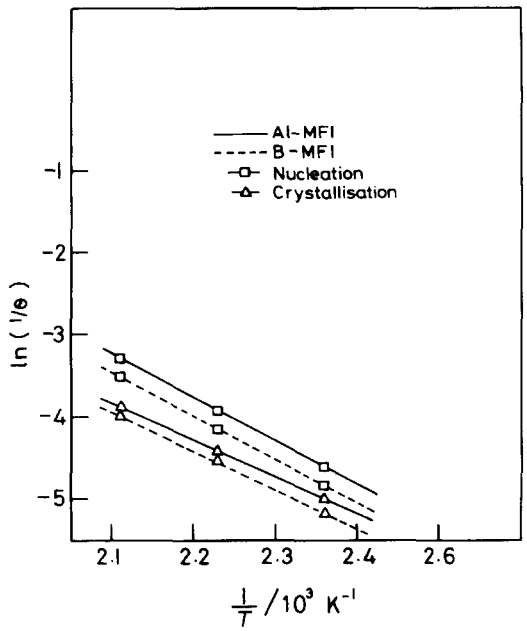

Fig. 3. Arrhenius plots for nucleation and crystallization of B-ZSM-5 and Al-ZSM-5 systems.

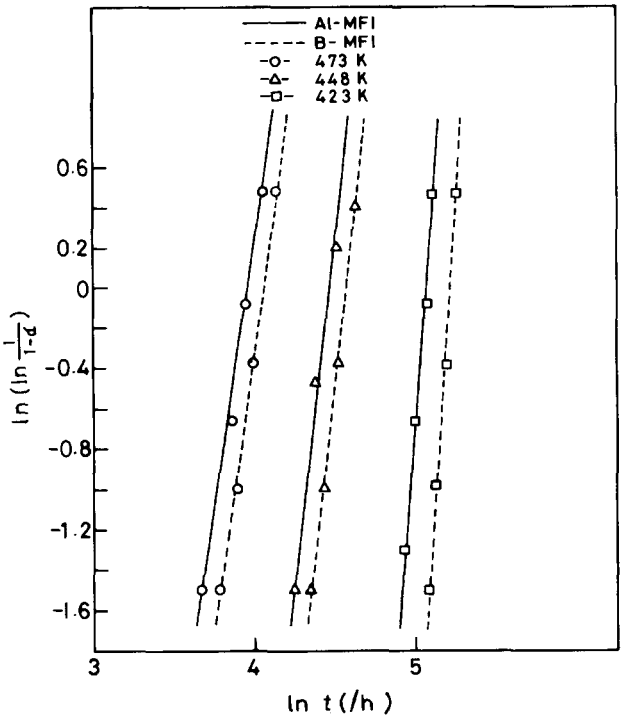

Fig. 4. Avrami-Erofeev plots for B-ZSM-5 and Al-ZSM-5 systems.

and crystallization must occur slower with the B-MFI system than with the Al-MFI system. These are apparent and not real values of E_n and E_c, because they are functions of many synthesis parameters, such as the synthesis time, temperature, pH, source of raw materials, etc. However, these values are comparable with those reported for the crystallization of ZSM-5 in the TPA system[23,26–28] in the literature.

Kinetics of Nucleation and Crystallization. It was shown that the process of zeolite nucleation and crystallization represented by sigmoid curves, such as that of shown in Fig. 2, can be described mathematically by the Avrami–Erofeev equation,[27,28]

$$\ln [1/(1-\alpha)] = (kt)^m, \quad (3)$$

where α and t are the fractional conversion and reaction time, respectively, and k and m are rate constants. The data of Fig. 2 were fitted to Eq. 3 and linear plots of $\ln(t)$ vs. $\ln[1/\ln(1-\alpha)]$, from which the calculated values of m and k are given in Fig. 4. The values of k and m obtained from these linear plots are compared and listed in Table 2. The salient feature of Table 2 is in accordance with the thermodynamic expectation of a decrease in k and an increase in m as the temperature of the zeolite synthesis decreases. The increase in k indicates a faster rate of nucleation, and the decrease in m signifies faster crystallization.[25] Table 2 shows that the values of k obtained for the Al-ZSM-5 system are higher than those of B-ZSM-5. This clearly indicates a faster rate of nucleation in the case of

Table 2. Avrami–Erofeev Parameters

Reaction temperature / K	m		$k \times 10^3$	
	B-ZSM-5	Al-ZSM-5	B-ZSM-5	Al-ZSM-5
423	11.9	9.5	5.5	6.3
448	7.2	6.4	10.6	11.6
473	5.6	4.8	17.1	18.7

the Al-ZSM-5 system. Similarly, a lower value of m in the case of Al-ZSM-5 than those with B-ZSM-5 indicates faster crystallization of Al-ZSM-5. The power m stands for the sum of two other constants, one indicating the number of stages in the nucleation process and the other indicating the number of directions in which crystal-growth propagation occurs. The values of m, assuming that the number of directions in which the crystal growth propagation occurs viz., shape of the crystal, are the same (Fig. 5) in both crystallization processes, reveal that the number of stages leading to stable nuclei of a size stable enough not to redissolve, but to grow into a crystal, are supposed to be more in the case of B-ZSM-5 than those leading to stable Al-ZSM-5 nuclei formation, due to less stability of BO_4 tetrahedra compared with AlO_4 tetrahedra in the secondary building unit.

Scanning Electron Microscopy and Chemical Analysis. Scanning electron micrographs of intermediates of both systems taken at intervals of the crystallization process at 448 K are shown in Fig. 5. In the initial stages of (untill 60 h of heating) crystallization of a gel mixture, only the amor-

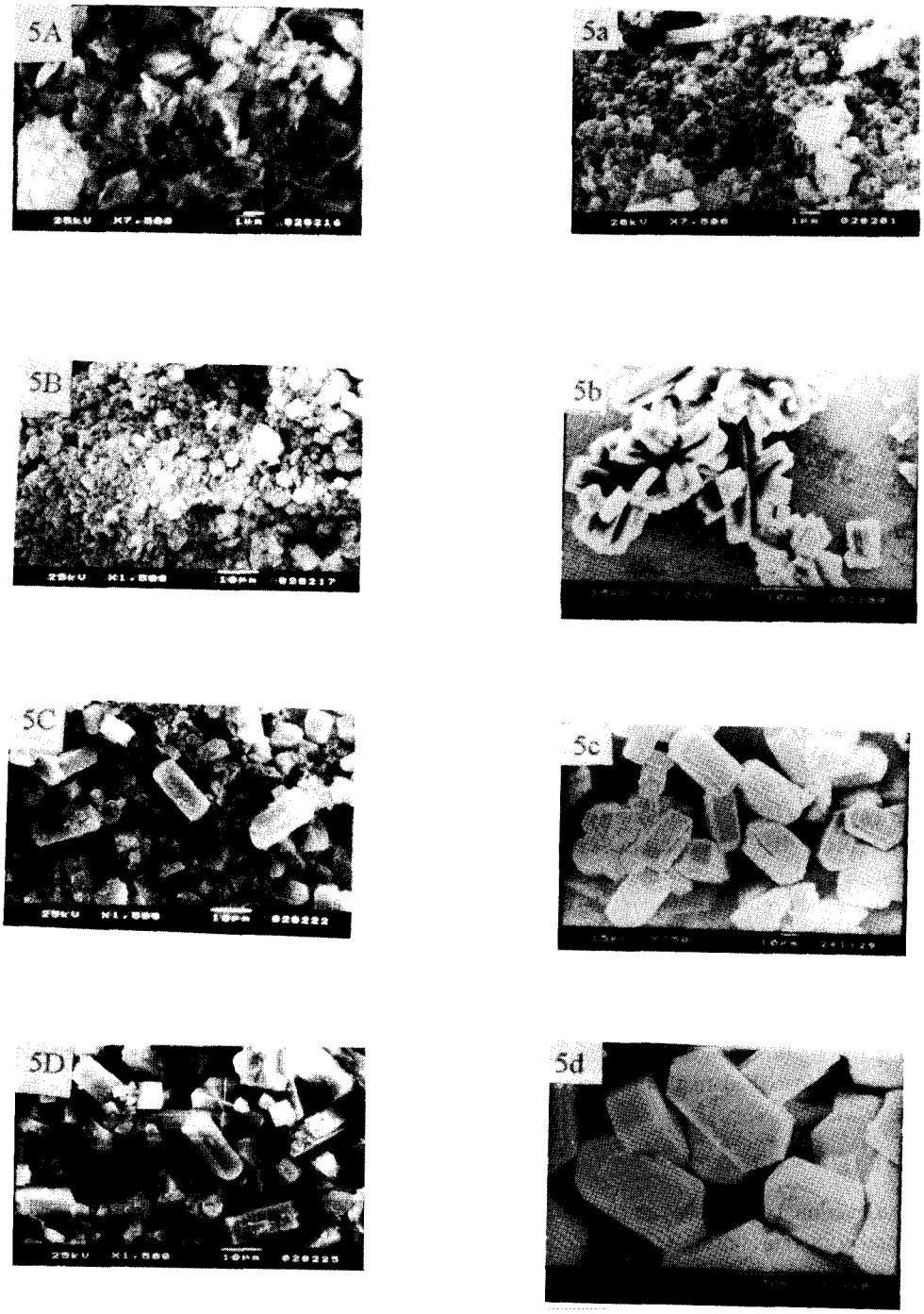

Fig. 5. SEM pictures of B-ZSM-5 and Al-ZSM-5 systems of crystallization at 448 K. B-ZSM-5 at 60 h (5A), 70 h (5B), 95 h (5C), 135 h (5D), and Al-ZSM-5 at 40 h (5a), 60 h (5b), 80 h (5c), and 120 h (5d).

phous phase is present, as evident from Fig. 5A. Figure 5B shows slightly developed crystals at 70th h. The coexistence of amorphous with crystalline phases (60% crystallization) is clear in Fig. 5C, which represents the intermediate drawn at 95th h. Figure 5D shows better outlined crystals of hexagonal shapes; these crystals are drawn at 135th h. Similar shaped, but always larger sized, crystals are observed for the Al-MFI system, as shown in pictures Figs. 5a, 5b, 5c, and 5d representing intermediates drawn at 40 h, 60 h, 85 h, and 120 h, respectively, during the crystallization period. The hexagonal nature of the crystals is attributed to the controlled or limited directional growth occurring in the B-MFI system, similar to the Al-MFI system of the same SiO_2/M_2O_3 ratio of the starting gel, but without any secondary growth over them.

Table 3 contains details of the chemical analysis of the intermediates and final products of both systems, taken at various time intervals of the crystallization process at 448 K. The SiO_2/M_2O_3 ratio (though different for the boron and aluminium systems) of the intermediates remains almost constant during crystal growth throughout the crystallization period. This shows that both systems crystallizes by the solid–solid transformation mechanism, which involves the rapid formation of innumerable nuclei, and consequently microcrystallites of zeolite due to the interaction of template molecules with metallosilicate hydrogels.[29] The amount of TBP in the solid increases with the crystallinity in the B-ZSM-5 system due to an increase of microcrystallites of zeolites with an increase of time. A large amount of TBP was already present at low X-ray crystallinity, and was constant with time in the case of Al-ZSM-5. This shows that a large number of microcrystallites are formed even at low crystallinity in the Al-ZSM-5 system, probably is due to the greater stability of Al containing a secondary building unit. From Table 3 it is further observed that a phosphorous residue is retained in channels of zeolites after calcination in both systems. The phosphorous residue of different amounts in the zeolite channel may enhance the shape selectivity of the products of reactions that may be catalyzed by M-ZSM-5 (M = Al or B), due to space constraints and acidity change. The change in crystallinity after calcination shows the release of boron from the zeolite framework due to a thermal instability. Thus, the change in the SiO_2/B_2O_3 ratio during calcination is due to deboronation of B-ZSM-5 at higher temperature.

Infrared Spectroscopy. The B-ZSM-5 and Al-ZSM-5 pentasil zeolite spectra, best observed for self-suported wafers with respect to KBr pellets, were compared (Fig. 6). In both cases, the IR spectra were typical of pentasil the zeolite. The well-defined IR bands at 800 and 450 cm^{-1} and the saturated region 1000—1300 cm^{-1} are characteristics of the SiO_4 tetrahedral, while the vibrational band at 550 cm^{-1} confirms the presence of five-member rings of the pentasil structures. A new band observed for the B-ZSM-5 system

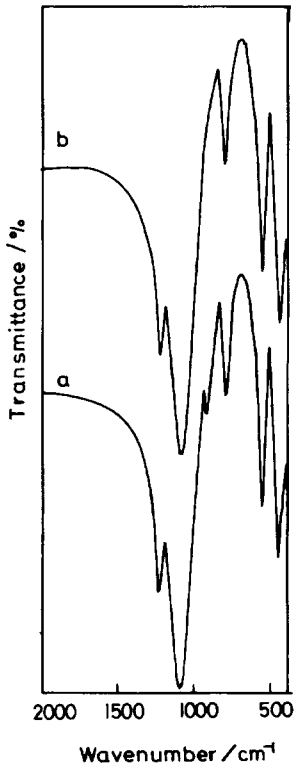

Fig. 6. Infrared spectra of a) B-ZSM-5, b) Al-ZSM-5.

Table 3. Composition of the Intermediates and the Final Products

System	% Crystallinity	SiO_2 mol %	M_2O_3 mol %	SiO_2/M_2O_3	TBP mol %	H_2O mol %
B-ZSM-5	10	85.3	1.35	63.2	0.84	7.28
	35	86.2	1.39	62.0	1.08	6.16
	69	87.9	1.43	61.5	1.29	5.75
	100	87.8	1.49	58.9	1.48	4.96
	78[a)]	94.2	0.67	140.6	0.82[b)]	—
Al-ZSM-5	15	76.1	0.95	80.1	1.29	5.78
	35	76.8	0.94	81.7	1.33	5.32
	79	77.5	1.0	77.5	1.38	5.05
	100	77.8	0.98	79.4	1.42	4.78
	96[a)]	86.4	0.97	89.0	0.78[b)]	—

a) Calcined at 823 K for 5 h in air. b) mol % of phosphorous after calcination.

Table 4. Reaction Time and IR Crystallinity

System	Reaction time/h	IR crystallinity A_{550}/A_{450}	% XRD crystallinity
B-ZSM-5	45	0.15	0
	80	0.30	20
	90	0.40	50
	135	0.78	100
Calcined B-ZSM-5		0.65	78
Al-ZSM-5	40	0.20	0
	80	0.38	30
	90	0.70	80
	120	0.80	100

at 920 cm^{-1} can be assigned to the presence of the tetra-coordinated framework boron, and is observed in all boron pentasils.[12,19] However, for a calcined boron sample a strong band also appears at 1380 cm^{-1}, which can be assigned to tricoordinated-framework boron.[12,19] The transformation of the absorption band at 920 cm^{-1} to one at 1380 cm^{-1} upon calcination is logically assigned to a change of boron coordination from tetrahedral to trigonal.

The intensity ratio (A_{550}/A_{450}) of the double-ring vibration and the 450 cm^{-1} band of the SiO_4 bending may be used as a measure of the crystallinity of zeolites. Table 4 shows that the A_{550}/A_{450} values were found to increase linearly with the degree of crystallinity of both systems. The IR spectroscopic technique was not dependent on the thershold partical size, because the X-ray diffraction technique is used to examine the micro structure of the precrystalline solid phase. The band observed at 550 cm^{-1} was tentatively assigned to the presence of such substructural units as a double 5 ring. Table 4 indicates the presence of microcrystallites of ZSM-5 precursors in apparently amorphous materials.

Conclusion

TBP acts as a structure-directing agent during nucleation by arranging silica tetrahedra in an orderly manner and leaves a phosphorous residue of different amounts in the zeolite channel after calcination in both cases. The phosphorous residue may offer better shape selectivity of the products. The slow rate of nucleation and crystallization of B-ZSM-5 results in simillar-shaped, but smaller sized, crystals and the incorpotration of a greater number of boron atoms compared to aluminum in the framework. The uniformity of the resulting crystals has the advantage of exibiting uniform catalytic activity and selectivity of the products.

References

1 R. M. Barrer, "Hydrothermal Chemistry of Zeolite," Academic Press, New York (1982), Chap. 6, p. 287.
2 R. M. Dessau and G. T. Kerr, *Zeolite*, **4**, 315 (1984).
3 D. Chang, C. T-W. Chu, J. N. Miale, R. F. Bridger, and R. B. Calvert, *J. Am. Chem. Soc.*, **106**, 8143 (1984).
4 M. Taramasso, G. Perego, and B. Notari, "Proc. 5th Int. Conf. Mol. Sieves," Heyden, London (1980), p. 40.
5 Z. Gablica, B. J. Nagy, P. Budart, and G. Debras, *Chem. Lett.*, **1984**, 1059.
6 Z. Gablica, B. J. Nagy, and G. Debras, *Stud. Sur. Sci. Catal.*, **19**, 113 (1984).
7 K. F. M. G. J. Scholle, A. P. M. Kentgens, V. S. Veeman, P. Frenken, and G. P. M. Van der Velden, *J. Phys. Chem.*, **88**, 5 (1984).
8 M. W. Simson, S. S. Nam, W. Xu, S. L. Suib, J. C. Edwards, and C. L. O'Young, *J. Phys. Chem.*, **96**, 6381 (1992).
9 J. Datka and M. Kawalex, *J. Chem. Soc., Faraday Trans. 1*, **89**, 1829 (1993).
10 J. C. Vedrine, *Stud. Surf. Sci. Catal.*, **1991**, 69.
11 L. Kubelkova, I. Jirka, J. Vylita, and J. Novakova, *Stud. Surf. Sci. Catal.*, **84**, 1051 (1994).
12 G. Coudurier, A. Auroux, J. C. Vedrine, R. D. Farlee, L. Abrams, and R. D. Shannon, *J. Catal.*, **108**, 1 (1987).
13 B. P. Liliana, A. A. Oscar, and A. O. Oscar, *Lat. Am. Appl. Res.*, **25**, 223 (1995).
14 N. Lingappan and V. Krishnasamy, *Bull. Chem. Soc. Jpn.*, **69**, 1 (1996).
15 A. Cichocki, M. Michalik, and M. Bus, *Zeolite*, **10**, 577 (1990).
16 S. A. Axon and J. Klinowski, *J. Phys. Chem.*, **98**, 1929 (1994).
17 D. Trong On, S. Kaliaguine, and L. J. Bonneviot, *J. Catal.*, **157**, 235 (1995).
18 U. Cornaro and B. W. Wojciechowski, *J. Catal.*, **120**, 182 (1989).
19 M. B. Sayed, A. Auroux, and J. C. Vedrine, *J. Catal.*, **116**, 1 (1989).
20 L. H. Hsing and C. L. O'Young, *Chem. Ind. (Dekker)*, **74**, 15 (1998).
21 D. Bianchi, M. W. Simon, S. S. Nam, W. Xu, S. L. Suib, and C. L. O. Young, *J. Catal.*, **145**, 551 (1994).
22 E. Dumitriu, D. T. On, and S. Kaliaguine, *J. Catal.*, **170**, 150 (1997).
23 S. Mintova, V. Valtchev, E. Vulcheva, and S. Veleva, *Zeolite*, **12**, 210 (1992).
24 A. N. Kotasthane, V. P. Shiralkar, S. G. Hedge, and S. B. Kulkarni, *Zeolite*, **6**, 253 (1986).
25 P. N. Joshi, G. N. Rao, A. N. Kotasthane, and V. P. Shiralkar, *J. Inclusion Phenom. Mol. Recognition Chem.*, **9**, 91 (1990).
26 N. Lingappan and V. Krishnasamy, *Cryst. Res. Technol.*, **31**, 275 (1996).
27 Z. Gabelica, M. C. Bierman, P. Boudart, A. Gourgue, and J. B. Nagy, *Stud. Surf. Sci. Catal.*, **24**, 55 (1985).
28 K. L. Chao, T. C. Tasi, M. S. Chen, and I. Wang, *J. Chem. Soc., Faraday Trans. 1*, **77**, 547 (1981).
29 M. J. Avrami, *Chem. Phys.*, **9**, 177 (1941).
30 B. V. C. R. Erofeev, *Acad. Sci. USSR*, **52**, 177 (1941).
31 S. P. Zhdanov, *ACS Adv. Chem. Ser.*, **101**, 20 (1971).